Processing and Application of Ceramics 12 [3] (2018) 209–217
https://doi.org/10.2298/PAC1803209A

Optical properties of annealed $As_{30}Te_{67}Ga_3$ thin films grown by thermal evaporation

Alaa M. Abd-Elnaiem*, Samar Moustafa

Physics Department, Faculty of Science, Assiut University, Assiut 71516, Egypt

Received 10 November 2017; Received in revised form 25 April 2018; Accepted 11 July 2018

Abstract

Chalcogenide glasses have received lots of attention because of their superior optical properties. To optimize these properties and expand areas of applications, more studies are required to establish the extent to which the parameters can be tuned over a wide range of annealing temperatures and heating rates. To do this, bulk and thin ~150 nm $As_{30}Te_{67}Ga_3$ films were prepared by melt-quenching and thermal evaporation techniques, respectively. The phase transition was investigated using differential scanning calorimeter (DSC) while the crystal structures were studied by X-ray diffraction (XRD). Characteristic temperatures such as the glass transition, crystallization and melting temperature of the bulk glass were found to depend on the heating rate. The activation energy of glass transition was 167.29 kJ/mol while the energy of crystallization was 103.98 kJ/mol. XRD results indicated that the annealed films showed more crystallinity, larger average crystallite size, lower dislocation density and lower strain as annealing temperature increased. According to the Avrami exponent, a combination of two and three-dimensional crystal growth with heterogeneous nucleation are possible mechanisms for the crystallization process. Moreover, optical constants such as the optical band gap, refractive index, extinction coefficient, high-frequency dielectric constants, real and imaginary parts of dielectric constants were found to strongly depend on the annealing temperature. The optical energy gap decreased from 1.1 to 0.89 eV as the annealing temperature increased from 373 to 433 K. These results indicate that thermal annealing is a major factor that can be used to tune the crystal structure, and hence the optical properties of $As_{30}Te_{67}Ga_3$ system.

Keywords: *As-Te-Ga chalcogenides, thin films, thermal annealing, structure, optical parameters*

I. Introduction

Chalcogenide glasses have received lots of attention because of their potential uses in optical fibers, infrared optical elements, optical transmission media, reversible phase change optical records among others [1,2]. These applications are premised on their superior optical and physical properties. Binary As-Te is archetypical chalcogenide glass-forming system with high crystallization ability [3]. Their properties can be improved significantly by adding other elements. Studies have shown that the addition of Ga to As-Te alloy is preferable for applications such as memory electrical switching devices [4]. Moreover, As-Te-Ga system can change phase from amorphous to crystalline and *vice versa* making it a promising candidate for optoelectronic applications [5]. Interestingly, the structures and consequently the optical properties of chalcogenide materials can be tuned by thermal annealing [6].

Studies on optical properties of As-Te-Ga are limited [5–7]. For instance, Dongol [7] reported that the addition of Ga influences the optical band gap, the glass transition and crystallization temperature of $As_{30}Te_{70-x}Ga_x$. Similarly, Abd-Elrahman *et al.* [5] found that as-prepared $Te_{67.5}Ga_{2.5}As_{30}$ thin film shows an indirect allowed transition with a decrease in the value of the optical energy gap as the thickness increases. Conversely, samples annealed at temperatures beyond the crystallization temperature show a direct allowed transition in which the optical energy gap increases with annealing temperature. In another publication, Abdel-Rahim [6] reported that the optical gap of $Ga_8As_{46}Te_{46}$ thin films increases with the annealing temperature up to 443 K. This, however, decreases sharply for higher tempera-

* Corresponding authors: tel: +20 88 2412229,
e-mail: *abd-elnaiem@aun.edu.eg*

ture. The observed change in the optical gap, as influenced by the thickness and the annealing temperature (up to 443 K) was interpreted based on the density of states model proposed by Mott and Davis [8].

Since reports on As-Te-Ga film are limited, this paper presents a more detailed experimental study on the influence of annealing temperature on the structural and optical parameters of $As_{30}Te_{67}Ga_3$ thin film. We conducted the study over a wide range of heating and annealing temperatures. In addition, the calorimetric study was conducted on the bulk samples to examine the glass transition and melting temperature. It should be noted that the composition of the film was intentionally chosen to lie within the glass-forming region to enable more understanding of the optical properties for more applications.

II. Experimental

Bulk $As_{30}Te_{67}Ga_3$ glasses were prepared by the conventional melt-quenching technique. High-purity As, Te and Ga (purchased from Sigma-Aldrich) were weighed accordingly and then inserted into a clean silica-glass ampoule. Then, the ampoule was sealed in a vacuum of 10^{-5} Torr and introduced into a furnace at 1100 K for 24 h. During the melting process, the ampoule was stirred continuously to ensure homogeneity of the melt. Finally, $As_{30}Te_{67}Ga_3$ bulk glass was obtained by quenching the ampoules in ice cold water. $As_{30}Te_{67}Ga_3$ thin films were then deposited on an ultrasonically cleaned glass substrate by thermal evaporation technique using a high-vacuum (10^{-5} Torr) coating unit (Model Edwards E306A). The film thickness (~150 nm) was determined using a quartz crystal thickness monitor.

The elemental compositions of the as-prepared bulk and thin films were examined by energy dispersive spectral X-ray spectroscopy (EDX). A Philips X-ray diffractometer type-1710 was employed to identify the crystalline phases in the samples. The crystallization kinetics was monitored by DSC (Model: TA - Q20). For this purpose, ~15 mg of the bulk glass sample was used. The measurement was performed under different heating rates (β) of 5–25 K/min and temperature range of 310–675 K. The glass transition temperature (T_g), crystallization extrapolated onset temperature (T_c), crystallization peak temperature (T_p) and melting temperature (T_m) were determined in this way. The thermal annealing of $As_{30}Te_{67}Ga_3$ thin films or bulk samples was conducted in a furnace under vacuum conditions at different temperatures for 1 h. The annealing process was carried out for the thin film samples at 373, 393, 413, 433, 473, and 513 K. The spectral transmittance (T) and reflectance (R) of the investigated films were measured using a computerized double beam spectrophotometer (Model: Shimadzu UV-2101) in the wavelength (λ) range from 300 to 2500 nm.

III. Results and discussion

3.1. Structural characterization

The EDX spectra of the as-prepared $As_{30}Te_{67}Ga_3$ bulk glass and thin films are shown in Figs. 1a and 1b. The peaks of As, Te, and Ga are clearly identified, and the atomic percentage compositions were calculated to be 30.38, 66.73 and 2.89, respectively. According to the XRD spectrum (Fig. 2), the as-prepared film, just as the bulk samples, is largely amorphous with a single peak at $2\theta = 72°$. This is attributed to the crystallization of As phase during preparation. Conversely, the samples annealed at 433, 473 and 513 K show few crystalline peaks which correspond to the orthorhombic, monoclinic and hexagonal crystal structure of As, As_2Te_3, and Ga_2Te_3 phases, respectively. Panish [9] reported a similar observation for other compositions of As, Te, Ga systems. Furthermore, it is clearly noted that the number and intensity of the crystalline peaks increased with annealing temperature. Based on the XRD data, we calculated the average crystallite size (D_{hkl}), interplanar distance (d_{hkl}), dislocation density (σ) and strain (ε) from Equa-

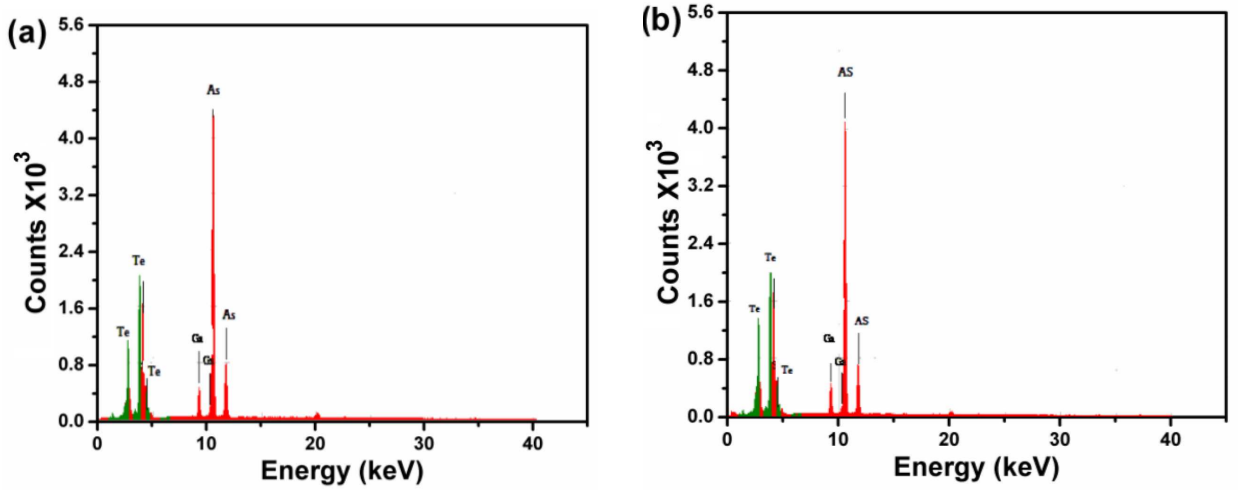

Figure 1. EDX for the as-prepared $As_{30}Te_{67}Ga_3$: a) bulk glass, and b) thin film

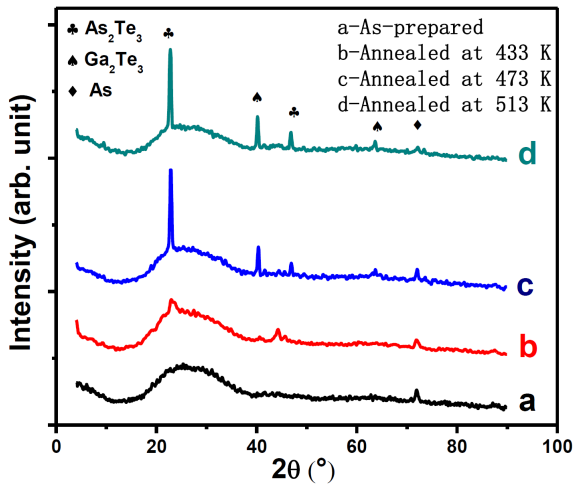

Figure 2. XRD data of the as-prepared and annealed $As_{30}Te_{67}Ga_3$ thin films

tions (1-4), respectively [11]. The results are presented in Table 1.

$$D_{hkl} = \frac{0.9\lambda}{\beta_{hkl}\cos\theta} \tag{1}$$

$$d_{hkl} = \frac{1}{\sqrt{\left(\frac{h}{a}\right)^2 + \left(\frac{k}{b}\right)^2 + \left(\frac{l}{c}\right)^2}} \tag{2}$$

$$\sigma = \frac{s}{D_{hkl}^2} \tag{3}$$

$$\varepsilon = \left(\frac{\lambda}{D_{hkl}\cos\theta} - \beta_{hkl}\right)\frac{1}{\tan\theta} \tag{4}$$

where λ is the X-ray wavelength, β_{hkl} is the full-width at half maximum, θ is the diffraction angle, h, k, and l are the Miller indices; a, b, and c are the lattice parameters and s is a factor, which equals unity for minimum dislocation.

According to Table 1, while average crystallite size increased with annealing temperature, the dislocation density and strain decreased accordingly. This observation indicates improved crystallinity due to the heat treatment which agrees with studies reported on some other chalcogenide thin films [11–13]. Figure 3a shows the DSC curves of $As_{30}Te_{67}Ga_3$ glass at different heating rates (from 5 to 25 K/min). Four characteristic phenomena were observed at different temperature regions. The first phenomenon is the endothermic peak corresponding to the glass transition temperature (T_g) while the second one corresponds to the crystallization onset temperatures (T_{c1} and T_{c2}). The third phenomenon is the crystallization exothermic peaks (T_{p1} and T_{p2}) while the last feature is the endothermic peak due to the melting (T_m). The values of these characteristic temperatures are given in Table 2. The observed melting point, 622 ± 0.5 K, is in agreement with the melting point of As_2Te_3 phase reported elsewhere [9]. Also, the existence of Ga shifts other characteristic temperatures by about 5 K compared to the $As_{30}Te_{70}$ system [12]. The values of T_g, T_{c1}, T_{c2}, T_{p1}, and T_{p2} increased with the heating rate. The appearance of double crystallization peaks at T_{c1} and T_{c2} (Fig. 3a) has been observed for many chalcogenide glasses, and it is attributed to the occurrence of phase separation [13–16]. To confirm this, the DSC curve for the annealed sample is presented in Fig. 3b. The glass transition and the first crystallization peak disappeared while the second crystallization peak can be observed in the insert of Fig. 3b.

Different approaches have been used to analyze the dependence of the glass transition temperature T_g on heating rate β. Among them is the empirical equation suggested by Lasocka [17]:

Table 1. The observed and standard ASTM values of interplanar distances (d_{hkl}), calculated average crystallite size (D_{hkl}), dislocation density (σ) and strain (ε) for as-prepared and annealed $As_{30}Te_{67}Ga_3$ thin films

Sample	Phase	d_{hkl} observed [Å]	d_{hkl} ASTM [Å]	D_{hkl} [nm]	$\sigma \times 10^{15}$ [m^{-2}]	$\varepsilon \times 10^{-3}$
As-prepared	As	1.313	1.310	17.99	3.09	2.01
Annealed at 433 K	As_2Te_3	3.873	3.8745	27.78	1.29	1.3
	Ga_2Te_3	2.222	2.229	22.03	2.06	1.64
	As_2Te_3	2.046	2.0491	12.45	6.45	2.91
	As	2.046	2.0472	11.62	7.41	3.12
Annealed at 473 K	As_2Te_3	3.89	3.89	19.97	2.51	1.81
	Ga_2Te_3	2.236	2.235	24.18	1.71	1.5
	As_2Te_3	1.937	1.9372	21.53	2.16	1.68
	Ga_2Te_3	1.461	1.4602	30.41	1.08	1.19
	As	1.311	1.311	22.22	2.03	1.63
Annealed at 513 K	As_2Te_3	3.905	3.8996	19.66	2.59	1.84
	Ga_2Te_3	2.244	2.2402	23.20	1.85	1.56
	As_2Te_3	1.94	1.9402	21.47	2.17	1.69
	Ga_2Te_3	1.462	1.4601	34.78	8.27	1.04
	As	1.309	1.310	30.23	1.09	1.2

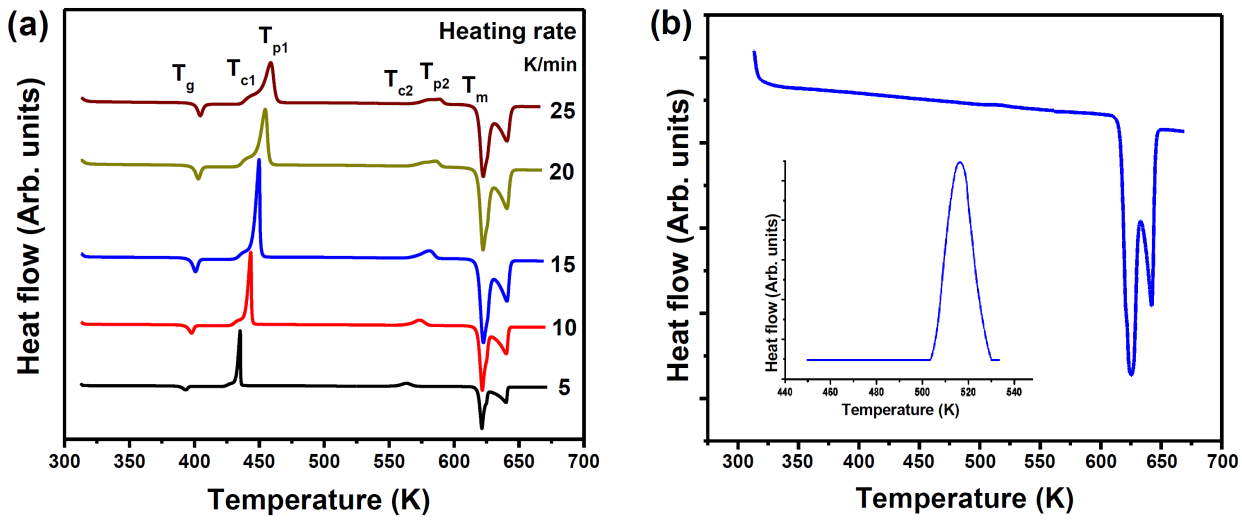

Figure 3. DSC traces for: a) $As_{30}Te_{67}Ga_3$ bulk glass at different heating rates (5–25 K/min) and b) annealed $As_{30}Te_{67}Ga_3$ bulk glass at 473 K for 1 h at heating rate 15 K/min

Table 2. The glass transition temperature (T_g), the onset crystallization temperatures (T_{c1} and T_{c2}), the crystallization peak temperatures (T_{p1} and T_{p2}), and the melting temperature (T_m) for $As_{30}Te_{67}Ga_3$ bulk glass at different heating rates

Heating rate [K/min]	T_g [K]	Peak 1		Peak 2		T_m [K]
		T_{c1} [K]	T_{p1} [K]	T_{c2} [K]	T_{p2} [K]	
5	389.12	422.23	435.24	554.23	563.76	621.45
10	393.24	426.94	443.44	563.22	573.64	621.75
15	397.96	431.32	449.89	567.12	582.02	622.59
20	400.32	434.21	454.96	565.89	585.42	622.33
25	401.21	434.99	458.92	469.32	588.32	622.44

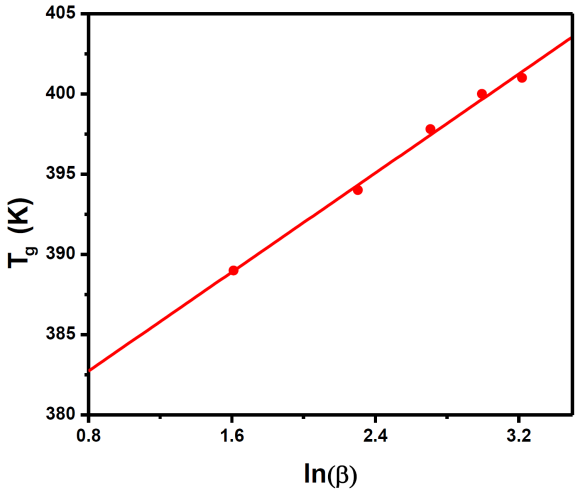

Figure 4. Plot of T_g versus lnβ for $As_{30}Te_{67}Ga_3$ bulk glass

$$T_g = A + B \cdot \ln\beta \tag{5}$$

where A and B are constants which depend on the glass compositions. The relationship between T_g and $\ln\beta$ for $As_{30}Te_{67}Ga_3$ is shown in Fig. 4 where A and B are calculated to be 18.3 and 375.96 K, respectively. Equation (5) can, therefore, be rewritten as:

$$T_g(\mathrm{K}) = 375.96 + 18.3 \ln\beta \tag{6}$$

The activation energy of glass transition (E_g = 167.29 kJ/mol) was obtained from Eq. (7) by plotting $\ln\beta$ against $1/T_g$ (Fig. 5a) [18,19]:

$$\ln\beta = \frac{E_g}{R \cdot T_g} + const. \tag{7}$$

Based on the first crystallization exothermic peak (T_{p1}), the activation energy of crystallization E_c can be obtained using the Kissinger's approach or the Johnson-Mehl-Avrami (JMA) model [20]:

$$\ln\frac{\beta}{T_{p1}^2} = -\frac{E_c}{R \cdot T_{p1}} + const. \tag{8}$$

The plot of $\ln(\beta/T_{p1}^2)$ versus $1/T_{p1}$ (Fig. 5b) yielded E_c of 103.98 kJ/mol. Additionally, the method suggested by Matusita *et al.* [21] for non-isothermal conditions can be employed here to describe the crystal growth process of the studied composition:

$$\ln[-\ln(1-\chi)] = n \cdot \ln\beta - 1.052\frac{m \cdot E_c}{R \cdot T} + const. \tag{9}$$

where χ is the conversion parameter, n is the Avrami exponent and m is an integer which depends on the mechanism of growth and crystal dimensionality. The value of the dimensional factor m is in the range of 1–3. The plot of $\ln[-\ln(1-\chi)]$ against $1/T$ at different heating rates (Fig. 6a) resulted to $m \cdot E_c$ of 577.87 kJ/mol from

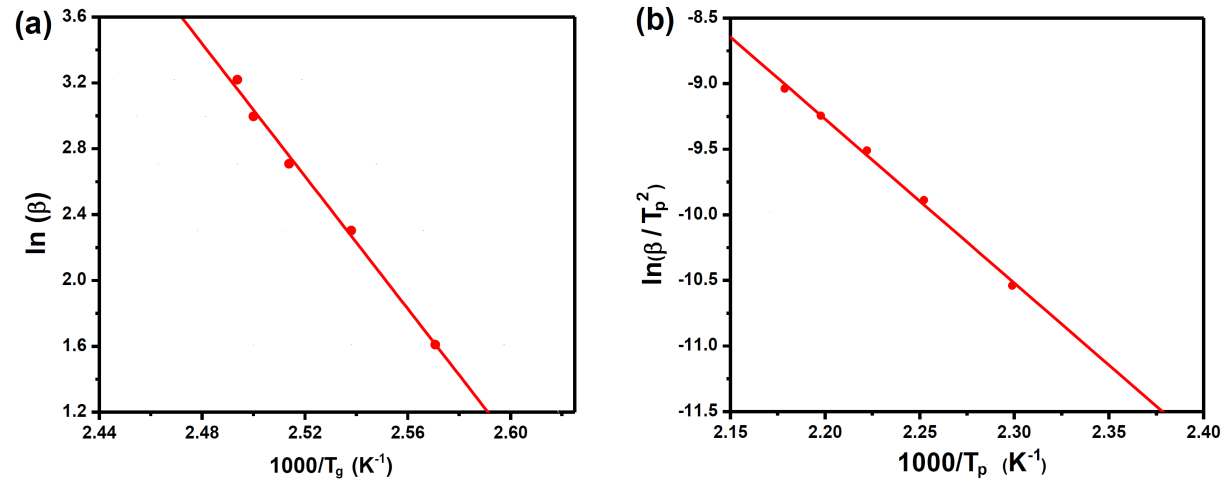

Figure 5. lnβ against 1000/T_g (a) and ln(β/T_{p2}) against 1000/T_p (b) for $As_{30}Te_{67}Ga_3$ bulk glass

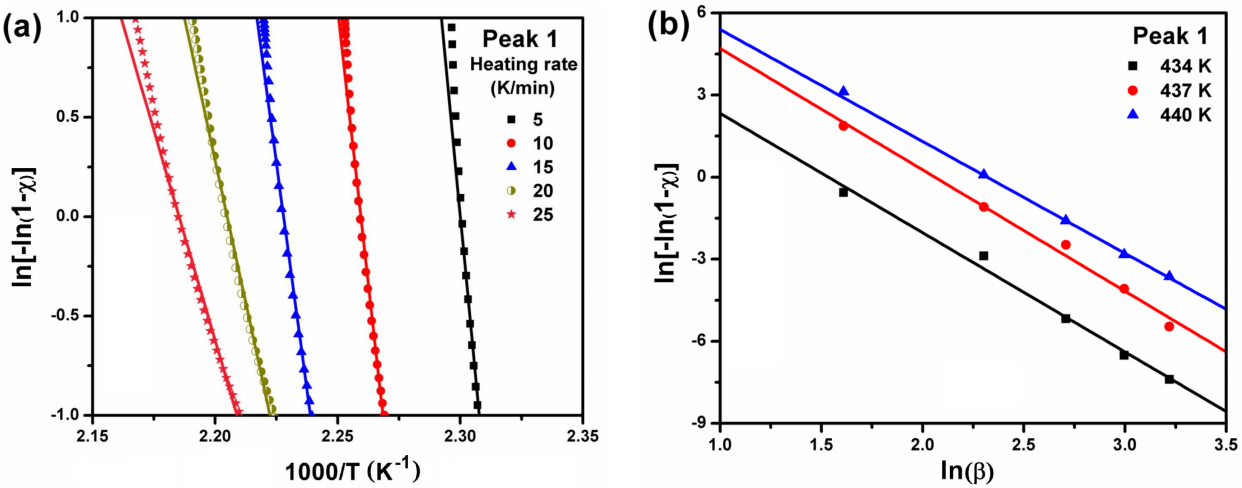

Figure 6. ln[−ln(1 − χ)] against 1000/T (a) and lnβ (b) at different temperatures for $As_{30}Te_{67}Ga_3$ bulk glass

where E_c and m were obtained as 103.98 kJ/mol and 5.5, respectively.

The Avrami exponent (n), which describes the crystal growth mechanism, is deduced from Eq. (10):

$$\left(\frac{\mathrm{d}\left[\ln\left(-\ln(1-\chi)\right)\right]}{\mathrm{d}(\ln\beta)}\right)_T = n \qquad (10)$$

The value of n (= m + 1) was obtained as 4.3 for all peaks from the plot of ln[− ln(1 − χ)] against lnβ (Fig. 6b). Since the value of n indicates that $m \approx 3$, more than one mechanism is involved in the crystallization process [22]. A good suggestion is a combination of two and three-dimensional crystal growth with heterogeneous nucleation [23].

3.2. Optical characterization

Figure 7a shows the dependence of transmittance (T) and reflectance (R) of $As_{30}Te_{67}Ga_3$ films on the annealing temperatures. It is clearly observed that T decreased with annealing temperature until 433 K, and increased thereafter. The decrease in the optical transmittance as a result of the thermal annealing may be due to the amorphous-crystalline transformation as observed from the XRD data and reported elsewhere [5,12,13,23]. Conversely, reflectance increased with annealing temperature at higher wavelengths. At lower wavelength, the variation of R with the annealing temperature is not clear.

Optical absorption

Absorption coefficient (α) is among the most relevant optical parameters for selecting good semiconductors. For a given film thickness d, α can be calculated from the reflectance and transmittance data using Eq. (11) [25]:

$$\alpha = \frac{1}{d}\cdot\ln\frac{(1-R)^2 + \sqrt{(1-R)^4 + 4\cdot(T\cdot R)^2}}{2\tau} \qquad (11)$$

The extinction coefficient (k) can thereafter be obtained from Eq. (12):

$$k = -\frac{\alpha\cdot\lambda}{4\pi} \qquad (12)$$

The extinction coefficient as a function of wavelength for $As_{30}Te_{67}Ga_3$ films at different annealing tempera-

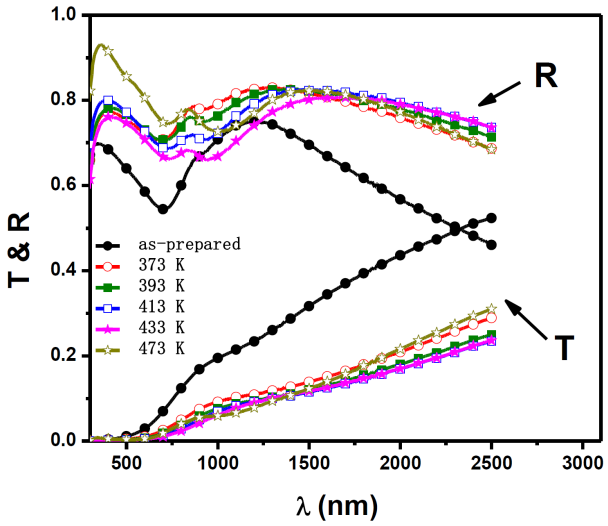

Figure 7. The transmittance (T) and reflectance (R) at different wavelengths (λ) for as-prepared and annealed $As_{30}Te_{67}Ga_3$ films

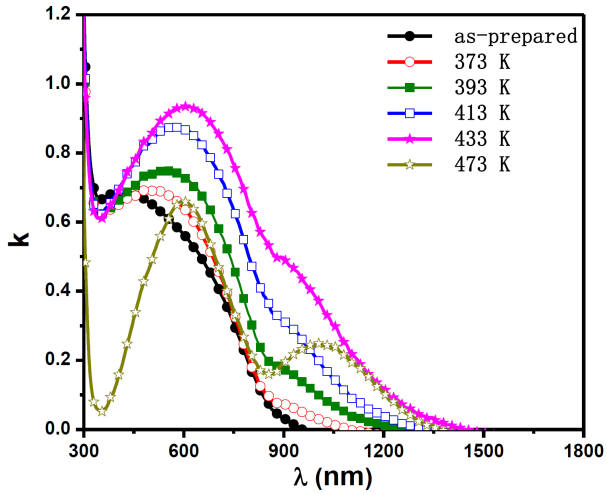

Figure 8. The relation between the extinction coefficient (k) and the wavelength (λ) of as-prepared and annealed $As_{30}Te_{67}Ga_3$ films

tures is shown in Fig. 8. It is observed that the value of k increased with annealing temperature up to 433 K and decreased thereafter. The increase in k may be attributed to the increase in the size of crystalline particles due to the thermal annealing effect. This is similar to the results of other chalcogenide thin films [5,13]. The decrease in k values for samples annealed at temperatures greater than 433 K could be attributed to the strain reduction (Table 1).

The band gap is obtained by analyzing the absorption data near the fundamental absorption edge. In most amorphous semiconductors, the variation of optical absorption as a function of the photon energy close to the fundamental absorption edge follows the exponential law. The common equation which is applied above the absorption tails is given in Eq. (13) [26]:

$$\alpha \cdot h \cdot \nu = B(h \cdot \nu - E_g)^r \tag{13}$$

where B is a constant and r is an index. According to the nature of electronic transition, r is proposed to have values of ½, ⅔, 2 and 3 for allowed direct transition, forbidden direct transition, allowed indirect transition and forbidden indirect transition, respectively [27]. For our samples, the index is $r = 2$ indicating the occurrence of indirect transitions. Furthermore, a plot of $(\alpha \cdot h \cdot \nu)^{1/2}$ against the photon energy $(h \cdot \nu)$ is linear (Fig. 9a), and therefore agrees with the classical theory of band to band transition. The indirect band gaps (E_g^{ind}) obtained from the intercepts of the straight lines in Fig. 9a, are summarized in Table 3. The decrease in indirect energy gap due to the thermal annealing at temperatures higher than T_g can be explained in terms of induced crystallization. In this case, weaker bonds are broken because of the existence of enough vibrational energy. Consequently, heat capacity is enhanced as more translational degrees of freedom are introduced into the system which results in decreased optical energy gaps [28]. The increase in the optical band gap above 433 K could be interpreted based on the Mott and Davis' model [8]. Accordingly, unsaturated defects are gradually annealed and density of localized states is reduced. This leads to an increased number of structure bands and consequently increases band gap [29].

Furthermore, the width of the localized states in the bandgap is an important optical parameter because it represents the degree of disorder in the semiconductor thin films [30]. This parameter can be determined from the Urbach's empirical relation [31]:

$$\alpha = \alpha_0 \cdot \exp\left(\frac{h \cdot \nu}{E_e}\right) \tag{14}$$

Table 3. Optical parameters for as-prepared and annealed $As_{30}Te_{67}Ga_3$ thin films

	As-prepared	373 K	393 K	413 K	433 K	473 K
E_g^{ind} [eV]	1.17	1.11	1.08	1.03	0.89	1.22
E_e [eV]	0.027	0.036	0.041	0.047	0.04 8	0.033
E_d [eV]	61.24	73.24	60.34	50.34	42.42	45.38
E_0 [eV]	2.53	2.44	2.45	2.34	2.31	2.42
ε_∞	83	356	420	500	479	420
λ_0 [nm]	360	369	378	397	381	433
$s_0 \times 10^{13}$ [m^{-2}]	29.50	69.45	69.84	57.92	55.98	95.37
$N/m^* \times 10^{57}$ [m^{-3}kg^{-1}]	11.29	49.04	55.84	60.06	61.48	62.91

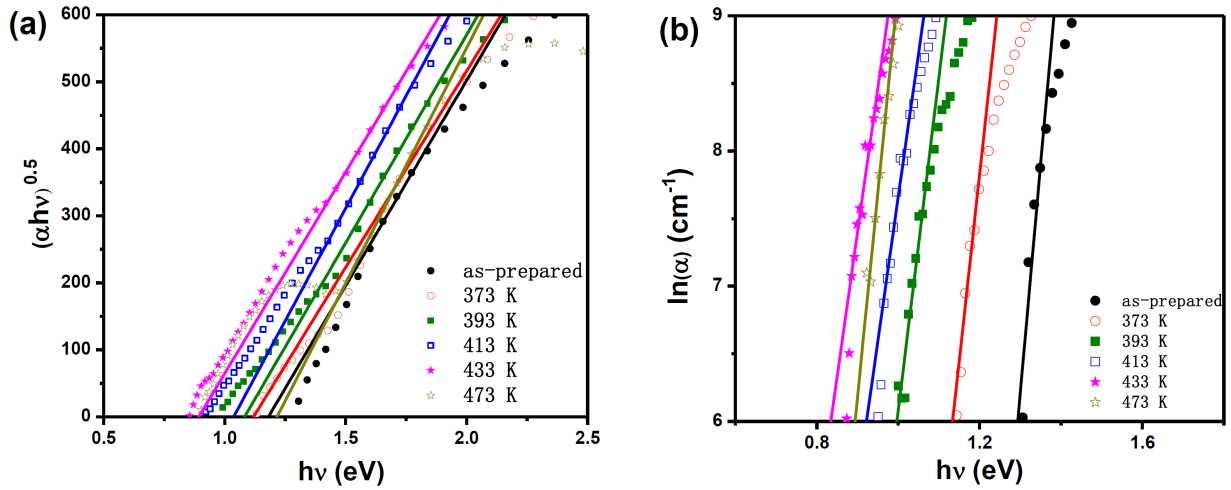

Figure 9. $(\alpha \cdot h \cdot \nu)^2$ **(a) and ln**α **(b) versus photon energy** $(h \cdot \nu)$ **for as-prepared and annealed** $As_{30}Te_{67}Ga_3$ **films (the straight lines are a linear fit of the Urbach tails)**

where α_0 is a constant and E_e is the band tail width. The plots of $\ln\alpha$ versus photon energy $(h \cdot \nu)$ for $As_{30}Te_{67}Ga_3$, at different annealing temperatures, are shown in Fig. 9b. The values of E_e obtained therefrom are listed in Table 3. The width of the localized states increased with temperature in the range of 373–433 K and decreased thereafter. The increase in the band tails width indicates higher disordered films due to the increased bandwidth of localized states. At annealing temperature above the crystallization temperature T_p, the crystallinity of the sample increases the width of the localized state thereby leading to an increased optical energy gap.

For a deeper understanding of the optical properties of $As_{30}Te_{67}Ga_3$ films, it is important to explore other optical parameters such as the refractive index, real and imaginary part of dielectric constant and high-frequency dielectric constant.

Dispersion parameters

The refractive index n is deduced from the reflectance R and the extinction coefficient k according to the following relation [32]:

$$R = -\frac{(n-1)^2 + k^2}{(n+1)^2 + k^2} \tag{15}$$

The values of the refractive index of $As_{30}Te_{67}Ga_3$ thin films at different annealing temperatures are plotted against the wavelength as shown in Fig. 10a. It is clear that n increases with increased annealing temperature within the range of 373–433 K and then decreases thereafter. The real component of the relative permittivity (ε') as a function of the wavelength (λ) is given by Eq. (16) [33]:

$$\varepsilon' = n^2 = \varepsilon_\infty - \frac{e^2}{4\pi \cdot c^2 \cdot \varepsilon_0} \cdot \frac{N}{m^*}\lambda^2 \tag{16}$$

where ε_∞ is the high-frequency dielectric constant, e the electronic charge, c the speed of light, ε_0 the permittivity of free space and N/m^* is the ratio of the carrier concentration N to the effective mass m^*. The value of ε_∞ was obtained from the linear plot of n^2 against λ^2 (Fig. 10b) at which $\lambda^2 = 0$. These values, tabulated in Table 3, indicated that high dielectric constant increased with

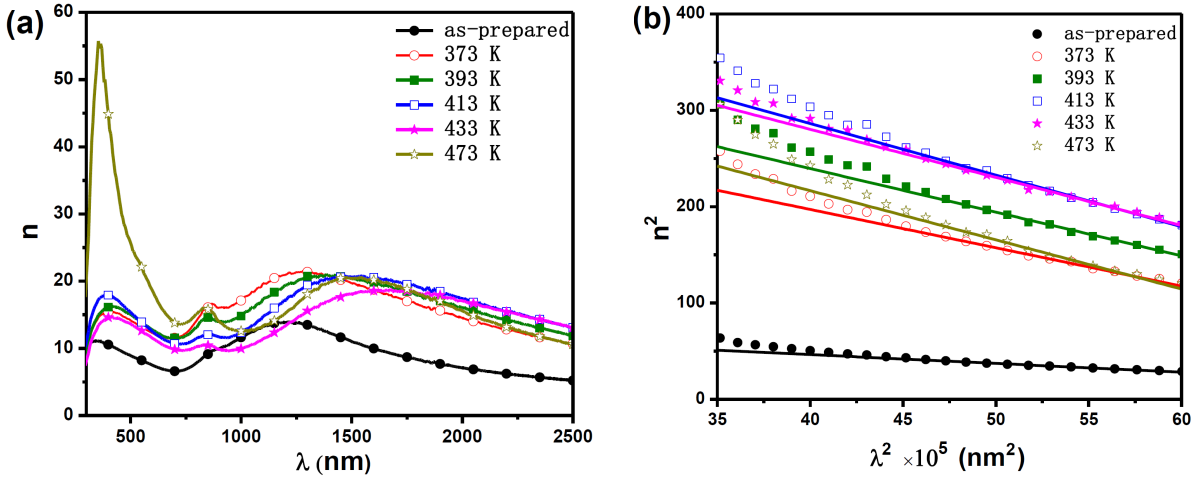

Figure 10. (a) refractive index (n**) versus wavelength (**λ**), and (b)** n^2 **versus** λ^2 **for as-prepared and annealed** $As_{30}Te_{67}Ga_3$ **films**

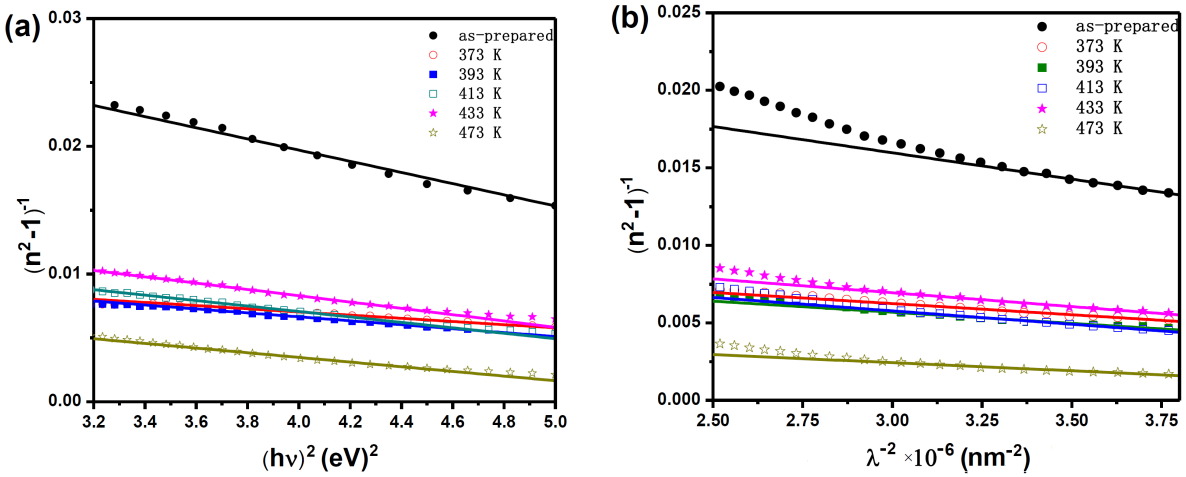

Figure 11. (a) plot of $(n^2-1)^{-1}$ versus $(h\cdot\nu)^{-2}$, and (b) $(n^2-1)^{-1}$ versus λ^{-2} for $As_{30}Te_{67}Ga_3$ films

annealing temperature within the range of 373–413 K and decreased thereafter. Similarly, the ratio N/m^* increased with annealing temperature, indicating that both ε_∞ and N/m^* could be attributed to the internal microstructure of the investigated composition.

The Wemple-DiDomenico (WDD) equation was employed to obtain the dispersion parameters of the films based on the single-oscillator approach [34] given as:

$$\frac{1}{n^2-1} = -\frac{E_0}{E_d} - \frac{1}{E_0\cdot E_d}(h\cdot\nu)^2 \qquad (17)$$

where E_0 and E_d are the single-oscillator fitting constants which measure the oscillator energy and strength of the interband optical transitions, respectively. Furthermore, E_0 is considered as an average energy gap, which scales with Tauc gap E_g, i.e. $E_0 = 2\times E_g$ [35]. By plotting $(n^2-1)^{-1}$ against $(h\cdot\nu)^2$ (Fig 11a), the values of E_0 and E_d were obtained from the slope and intersection of the straight lines. The values presented in Table 3 indicate that, within the measurement accuracy, the relation $E_0 = 2\times E_g$ [35] holds for this study. Generally, the variation of E_d with the annealing temperature is similar to that of E_g (Table 3). This indicates that the strength of the interband optical transition decreased with temperature from 373 to 433 K and increased thereafter. The phenomenon can be attributed to the change in the atomic diffusion within the annealed films giving more atoms at interstitial sites.

The refractive index data were also analysed to get the oscillator wavelength (λ_0) and the average oscillator strength (S_0) using the Sellmeyer's dispersion formula:

$$\frac{1}{n^2-1} = \frac{1}{S_0\cdot\lambda_0^2} - \frac{1}{S_0\cdot\lambda^2} \qquad (18)$$

The relation between $(n^2-1)^{-1}$ and λ^{-2} for the $As_{30}Te_{67}Ga_3$ film as a function of the annealing temperature is shown in Fig. 11b. The calculated values of λ_0 and S_0 are summarized in Table 3. These parameters are observed to increase with annealing temperature.

IV. Conclusions

The DSC results confirmed the glassy nature of $As_{30}Te_{67}Ga_3$ composition prepared by the melt-quenching method. Moreover, double crystallization peaks were observed which indicate a phase separation upon heating in the studied composition. The glass transition or crystallization temperatures were found to depend on the heating rate. Also, the XRD spectra showed not only the amorphous nature of the as-prepared films but also a polycrystalline structure for the annealed ones. The values of the indirect band gap were dependent on the annealing temperature. Moreover, the dispersion parameters are affected by thermal annealing, indicating the variation of the density of localized states of the studied annealed films. This shows that thermal annealing is a major factor that can be used to tune the crystal structure, and hence the optical properties of the $As_{30}Te_{67}Ga_3$ system.

References

1. R. Zallen, C.M. Penchina, "The physics of amorphous solids", *Am. J. Phys.*, **54** (1986) 862–863.
2. A. Burian, P. Lecante, A. Mosset, J. Galy, J.M. Tonnerre, D. Raoux, "Differential anomalous X-ray scattering studies of amorphous $Cd_{59}As_{41}$ and $Cd_{26}As_{74}$", *J. Non Cryst. Solids*, **212** (1997) 23–39.
3. H. Endo, H. Hoshino, H. Ikemoto, T. Miyanaga, "Semiconductor-metal transition in liquid As-Te mixtures", *J. Phys. Condens. Matter*, **12** (2000) 6077–6099.
4. S. Kim, H.-D. Kim, S.-J. Choi, "Intrinsic threshold switching responses in AsTeSi thin film", *J. Alloys Compd.*, **667** (2016) 91–95.
5. M.I. Abd-Elrahman, M.M. Hafiz, "On thickness and annealing dependence of optical properties of $Te_{67.5}Ga_{2.5}As_{30}$ thin film as optoelectronic material", *J. Alloys Compd.*, **551** (2013) 562–567.
6. M.A. Abdel-Rahim, "Annealing dependence of optical and electrical properties of $Ga_8As_{46}Te_{46}$ thin films", *J. Phys. Chem. Solids.*, **60** (1999) 29–39.
7. M. Dongol, "Optical absorption and structural properties of as-deposited and thermally annealed As-Te-Ga thin

films", *Egypt. J. Solids*, **25** (2002) 33–47.
8. N.F. Mott, E.A. Davis, *Electronic Processes in Non-Crystalline Materials*, Clarendon Press, Oxford, 1979.
9. M.B. Panish, "The ternary condensed phase diagram of the Ga-As-Te system", *J. Electrochem. Soc.*, **114** (1967) 91–95.
10. A.J.P. Wilson, *Mathematical Theory of X-ray Powder Diffractometry*, Cordon and Breach, New York, 1963.
11. A.M. Abd-Elnaiem, M. Mohamed, R.M. Hassan, M.A. Abdel-Rahim, A.A. Abu-Sehly, M.M. Hafiz, "Structural and optical characterization of annealed $As_{30}Te_{60}Ga_{10}$ thin films prepared by thermal evaporation technique", *Mater. Sci.-Poland*, **36** (2018) 193–202.
12. A.M. Abd-Elnaiem, M. Mohamed, R.M. Hassan, M.A. Abdel-Rahim, A.A. Abu-Sehly, M.M. Hafiz, "Influence of annealing temperature on the structural and optical properties of $As_{30}Te_{70}$ thin films", *Mater. Sci.-Poland*, **35** (2017) 335–345.
13. M.A Abdel-Rahim, A.Y. Abdel-Latief, M. Rashad, N.M. Abdelazim, "Annealing effect on structural and optical properties of $Se_{87.5}Te_{10}Sn_{2.5}$ thin films", *Mater. Sci. Semicond. Process.*, **20** (2014) 27–34.
14. M.A Abdel-Rahim, A.Y. Abdel-Latif, A.S. Soltan, "Structural study of chalcogenide $Ge_{20}Se_{50}Te_{30}$ glass", *Physica B Condens. Matter.*, **291** (2000) 41–48.
15. S. Asokan, G. Parthasarathy, E.S.R. Gopal, "Crystallization studies on bulk Si_xTe_{100-x} glasses", *J. Non Cryst. Solids*, **86** (1986) 48–64.
16. R.A. Ligero, J. Va, P. Villares, R. Jime, "Resolving overlapping peaks in differential scanning calorimetry", *J. Non Cryst. Solids*, **124** (1990) 63–70.
17. M. Lasocka, "The effect of scanning rate on glass transition temperature of splat-cooled $Te_{85}Ge_{15}$", *Mater. Sci. Eng.*, **23** (1976) 173–177.
18. A. Giridhar, S. Mahadevan, "Studies on the As-Sb-Se glass system", *J. Non Cryst. Solids*, **51** (1982) 305–315.
19. S. Mahadevan, A. Giridhar, A.K. Singh, "Calorimetric measurements on As-Sb-Se glasses", *J. Non Cryst. Solids*, **88** (1986) 11–34.
20. H.E. Kissinger, "Variation of peak temperature with heating rate in differential thermal analysis", *J. Res. Natl. Bur. Stand.*, **57** (1956) 217–221.
21. K. Matusita, T. Komatsu, R. Yokota, "Kinetics of non-isothermal crystallization process and activation energy for crystal growth in amorphous materials", *J. Mater. Sci.*, **19** (1984) 291–296.
22. M.A. Abdel-Rahim, A.Y. Abdel Latief, A. El-Korashy, M.A. El-Sattar, "Kinetic analysis of crystallization process in amorphous $Se_{90-x}Te_{10}Pb_x$ glasses", *Mater. Trans.*, **51** (2010) 428–433.
23. P.K. Jain, K.S. Rathore, N.S. Saxena, "Structural characterization and phase transformation kinetics of $Se_{58}Ge_{42-x}Pb_x$ (x = 9, 12) chalcogenide glasses", *J. Non Cryst. Solids*, **355** (2009) 1274–1280.
24. M.A. Abdel-Rahim, M.M. Hafiz, A.Y. Abdel-Latief, A.M. Abd-Elnaiem, A. Elwhab B. Alwany, "A study of the non-isothermal crystallization kinetic of $Zn_{10}Se_{90}$ glass", *Appl. Phys. A*, **119** (2015) 881–890.
25. J.I. Pankove, *Optical Processes in Semiconductors*, Dover Puble., New York, 2012.
26. J. Tauc, *Amorphous and Liquid Semiconductors*, Plenum Press, New York, 1974.
27. R.A. Smith, "Infra-red photo-conductors", *Adv. Phys.*, **2** (1953) 321–369.
28. A.S. Soltan, M. Abu El-Oyoun, A.A. Abu-Sehly, A.Y. Abdel-Latief, "Thermal annealing dependence of the structural, optical and electrical properties of selenium-tellerium films", *Mater. Chem. Phys.*, **82** (2003) 101–106.
29. M. Dongol, M. Abou Zied, G.A. Gamal, A. Ei-Denglawey, "The effects of composition and heat treatment on the structural and optical properties of $Ge_{15}Te_{85-x}Cu_x$ thin films", *Physica B Condens. Matter.*, **353** (2004) 169–175.
30. J.A Olley, "Structural disorder and the Urbach edge", *Solid State Commun.*, **13** (1973) 1437–1440.
31. F. Urbach, "The long-wavelength edge of photographic sensitivity and of the electronic absorption of solids", *Phys. Rev.*, **92** (1953) 1324–1324.
32. D. Hülsenberg, A. Harnisch, A. Bismarck, *Microstructuring of Glasses*, Springer, Berlin, 2008.
33. Z.H. Khan, M. Zulfequar, T.P. Sharma, M. Husain, "Optical properties of a-$Ga_{20}Se_{80-x}Sb_x$ thin films", *Opt. Mater.*, **6** (1996) 139–146.
34. S.H. Wemple, "Refractive-index behavior of amorphous semiconductors and glasses", *Phys. Rev. B*, **7** (1973) 3767–3777.
35. H. Ticha, L. Tichy, "Semiempirical relation between non-linear susceptibility (refractive index), linear refractive index and optical gap and its application to amorphous chalcogenides", *J. Optoelectron. Adv. Mater.*, **4** (2002) 381–386.